Progress In Electromagnetics Research C, Vol. 102, 13–30, 2020

Compact Dual-Band MIMO Antenna System for LTE Smartphone Applications

Haneen S. Aziz and Dhirgham K. Naji*

Abstract—The design of an eight-port MIMO antenna at the sub-6-GHz (LTE 42/43 and 46) bands for fifth-generation (5G) smartphone is presented. First, based on the Babinet's principle, a microstrip slot antenna (MSA) is designed from its counterpart complementary structure, microstrip patch antenna (MPA) to operate over the LTE 46 band. In order to make the MSA to operate at the specified three LTE bands, a proposed single antenna, namely RMSA, is achieved by adding a strip-ring resonator within the grounded slot of MSA which shows a good measured impedance bandwidth ($S_{11} \leq -6\,\text{dB}$) of $3.28 \sim 3.84\,\text{GHz}$ and $5.14 \sim> 6.0\,\text{GHz}$. Then, eight similar antenna elements of RMSA are printed on a smartphone printed circuit board (PCB). An FR4 substrate is used as the system PCB with an overall dimension of $80 \times 150 \times 0.8\,\text{mm}^3$. Two techniques, namely polarization and pattern diversity, are exhibited by designing the MIMO system due to the orthogonal arrangement of microstrip lines feeding the RMSAs. Simulated and experimental results are conducted to examine the performance of the designed MIMO antenna. Good isolation, acceptable gain, and efficiency are obtained over the bands of interest which verify the suitability of the proposed system for MIMO smartphone applications.

1. INTRODUCTION

In current and future mobile communications, there is noteworthy increased interest by researchers for multi-input-multi-output (MIMO) antenna systems [1]. This MIMO technology is an important component and certainly the most recently reported to realize antenna designs having better diversity performance and improved data throughput. Some of these MIMO antennas have been designed for Ultrawideband (UWB) wireless communications [2–5], long term evolution (LTE), and the fifth generation (5G) for smartphone applications [6–19]. However, restricted size of 5G smartphone devices remains a challenging task for antenna engineers in designing MIMO antenna systems having high-diversity performance with low envelope correlation coefficients (ECCs) among their ingredients of antennas. In standard MIMO systems, two or four antenna elements are used whereas in massive MIMO systems, a relatively high number ($N \geq 8$) of antennas are printed in the smartphone printed circuit board (PCB) [20]. In the literature, several 5G massive MIMO antenna designs have been proposed for improving their isolation characteristics by using dual- or tri-polarized antennas [7–9], decoupled building block method [10–13], neutralization line [14–16], self-isolated antenna element technique [17, 18], and orthogonal-mode mechanism [19].

Most of the previous designs are interested in single-band operations except for [11, 13, 15, 16], which consider dual-band antenna designs for 5G smartphone terminals operating below sub-6 GHz spectrum. It is noted that both the LTE 42/43 (3.4–3.8 GHz) and LTE 46 (5.150–5.925 GHz) are the standard bands dedicated to the future sub-6 GHz 5G systems [20–27].

Received 11 February 2020, Accepted 2 April 2020, Scheduled 13 May 2020
* Corresponding author: Dhirgham K. Naji (dhrgham.kamal@gmail.com).
The authors are with the Department of Electronic and Communications Engineering, College of Engineering, Al-Nahrain University, Baghdad, Iraq.

Different compact dual-band MIMO antenna designs have been reported in the literature. They are either applicable to general wireless communication applications [28, 29] or to smartphones but with number of MIMO antennas lower than four [30–32]. In particular, Ref. [32] addresses a 2×2 dual-band MIMO antenna system for mobile handset applications covering 1.9 and 2.45 GHz. The advances in 5G technology encourage researchers to go to higher frequencies and beyond 4-antennas MIMO system while keeping a simple design and implementation. This issue is addressed in this work.

The design of MIMO antenna arrays in dual-band operations is dedicated for sub-6 GHz 5G applications, and it is still a challenging task for researchers. The aim is to design dual-band MIMO antenna systems having better diversity characteristics and good radiation performances. Therefore, this paper presents a new design of an 8-antenna array with a compact and simple structure covering dual-band operations suitable for 5G smartphone applications. The theory of Babinet's principle is applied herein for designing the single antenna element, namely strip-ring shaped microstrip slot antenna (RMSA) from its counterpart complementary structure, microstrip patch antenna (MPA). This antenna element is successfully designed to operate at 3.5 and 5.5 GHz, a candidate resonant modes for LTE 42/43 and LTE 46 bands. Based on this antenna element, a dual-band 8-antenna MIMO system is presented. By arranging these antennas in orthogonal manner to share one printed circuit board (PCB), good diversity and isolation performance can be obtained. The proposed antenna element and the 8-antenna MIMO system are designed and analyzed using CST Microwave Studio. The simulated results in terms of S-parameters (reflection and transmission coefficients), antenna gains, and efficiencies besides radiation patterns are presented. Moreover, envelope correlation coefficient (ECC) and total active reflection coefficient (TARC) are also computed. Finally, prototypes of the designed antennas are fabricated, and an acceptable agreement between simulated and measured results is obtained.

2. DESIGN AND PERFORMANCE OF A SINGLE ANTENNA

2.1. Antenna Structure

The schematic of the proposed single antenna is illustrated in Fig. 1. As can be observed, the antenna is composed of a main slot radiator of dimensions $W_s \times L_s$ and a capacitively-coupled strip-ring resonator $W_r \times L_r$, and they are etched on the back side of an FR4 substrate of total dimensions $W_{sub} \times L_{sub}$ (18 mm $\times$ 18 mm) and (height h_{sub} of 0.8 mm, $\varepsilon_r = 4.3$, and tangential loss $\tan\delta = 0.025$). A microstrip line is printed on the front side of the substrate, for feeding the antenna structure, of dimensions $W_f \times L_f$ with $W_f = 2$ mm set to achieve input impedance of 50 Ω. Such a simple structure allows the antenna for easily having dual-band characteristic with resonance frequencies 3.5 and 5.5 GHz at the two bands suitably being used in the LTE 42/43 band (3.4–3.8 GHz) and LTE 46 band (5.150–5.925 GHz) for future smartphone applications. For correctly analysis and simulation of the antenna, the microstrip line is terminated by a sub-miniature-A (SMA) connector. A CST Microwave Studio tool is used for designing and optimizing the resonating antenna.

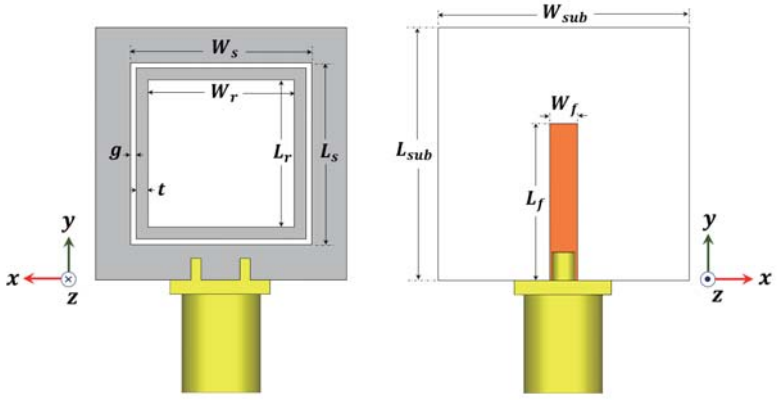

Figure 1. Layout of the proposed monopole antenna. (a) Back view. (b) Front view.

2.2. Evolution Steps of the Single Antenna

The antenna design procedure, namely, step 1 (Ant0), step 2 (Ant1), and step 3 (Ant2), is illustrated systematically in Fig. 2, and their optimized geometrical parameters are listed in Table 1. These three design steps are discussed in detail, and their reflection coefficient performances as a function of frequency is also shown.

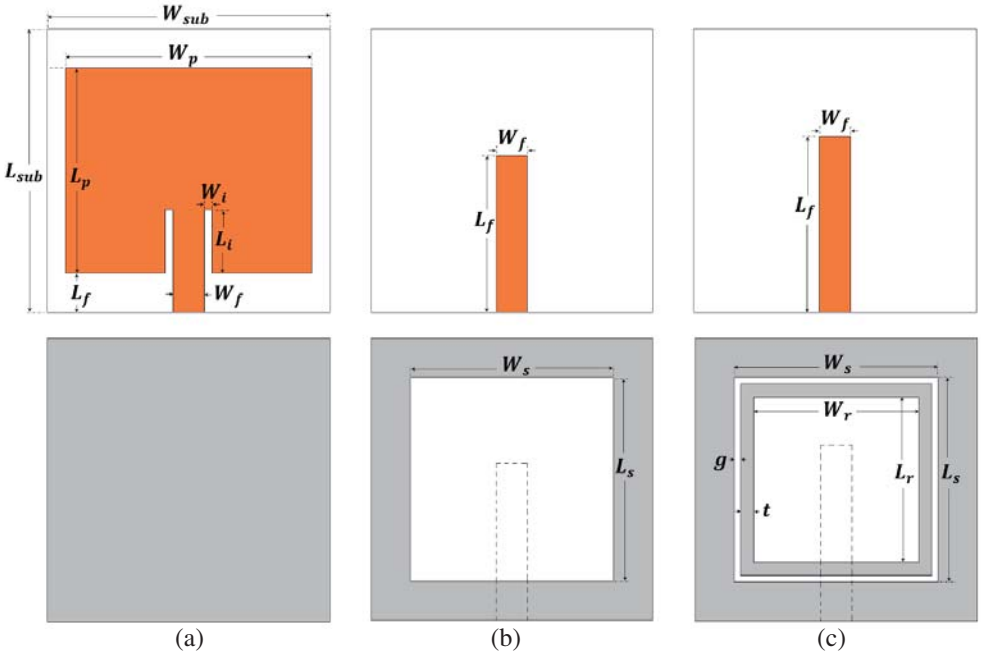

Figure 2. Geometrical design steps of the proposed single antenna, front view (in the upper part) and back view (in the lower part): (a) Ant0; (b) Ant1; (c) Ant2.

Table 1. The dimensions of the proposed three antennas.

Geometric parameter	Symbol	Value (mm)		
		Ant0	Ant1	Ant2
The substrate length	L_{sub}	18.0	18.0	18.0
The substrate width	W_{sub}	18.0	18.0	18.0
The substrate height	h_{sub}	0.8	0.8	0.8
The feedline length	L_f	2.5	10.0	11.2
The feedline width	W_f	2.0	2.0	2.0
The patch length	L_p	13.0	-	-
The patch width	W_p	15.7	-	-
The length of inset slot	L_i	4.0	-	-
The width of inset slot	W_i	0.5	-	-
The slot length	L_s	-	13.0	13.0
The slot width	W_s	-	13.0	13.0
The length of a square ring resonator	L_r	-	-	10.5
The width of a square ring resonator	W_r	-	-	10.5
The thickness of a square ring resonator	t	-	-	0.85
The gap between the slot and ring	g	-	-	0.4

Step 1 (Ant0): Initially, as the first design step for getting the optimized antenna with desired performance, an inset-fed microstrip patch antenna (MPA) considered as a reference antenna (RA), as depicted in Fig. 2(a), is designed by assuming that the following information is given: the desired resonance frequency (f_r), relative permittivity (ϵ_r), and the height of substrate (h_{sub}).

By using above information as antenna design parameters in the transmission line model (TLM), one can approximately find the patch width and length W_p and L_p, respectively as follows [33]:

$$W_p = \frac{\lambda_0}{2\sqrt{\varepsilon_{\text{rave}}}} = \frac{c}{2f_r\sqrt{\varepsilon_{\text{rave}}}} \tag{1a}$$

$$L_p \cong \frac{\lambda_0}{2\sqrt{\varepsilon_{\text{reff}}}} = \frac{c}{2f_r\sqrt{\varepsilon_{\text{reff}}}} - 2\Delta L_p \tag{1b}$$

where λ_0 and c are the free-space wavelength and velocity of light, respectively; $\varepsilon_{\text{rave}}$ and $\varepsilon_{\text{reff}}$ are the average and effective dielectric constant, respectively; and ΔL_p is the extended patch length, which are computed as:

$$\varepsilon_{\text{rave}} = \frac{\varepsilon_r + 1}{2} \tag{2a}$$

$$\varepsilon_{\text{reff}} = \frac{\varepsilon_r + 1}{2} + \frac{\varepsilon_r - 1}{2}\left(\frac{1}{\sqrt{1 + 12h_{sub}/W_p}}\right) \tag{2b}$$

$$\Delta L_p = 0.412h_{sub}\frac{(\varepsilon_{eff} + 0.300)}{(\varepsilon_{eff} - 0.258)}\frac{\left(\frac{W_p}{h_{sub}} + 0.262\right)}{\left(\frac{W_p}{h_{sub}} + 0.813\right)} \tag{2c}$$

As noticed in the above-mentioned TLM equations, to work at the dominant TM_{01} mode, the MPA patch width and length should be equal to $\lambda_0/2\sqrt{\varepsilon_{\text{rave}}}$ and slightly less than $\lambda_0/2\sqrt{\varepsilon_{\text{reff}}}$, respectively. Hence, by substitution in Eqs. (1) and (2), $f_r = 5.5\,\text{GHz}$ (LTE 46 band), $h_{sub} = 0.8\,\text{mm}$, and $\varepsilon_r = 4.3$, one can obtain $W_p = 16.75\,\text{mm}$ and $L_p = 12.40\,\text{mm}$.

Since the TLM approach is not accurate to give us the desired results, these two values of W_p and L_p (16.75 mm and 12.4 mm), respectively, are used as initial dimensions of the patch, which are applied at the first run of the simulation program. Then, by using the parametric sweeping technique through CST MWST for the antenna's geometrical parameters, the MPA is successfully designed for resonating at $f_r = 5.47\,\text{GHz}$ (with optimized patch size $W_p \times L_p$ of $15.7\,\text{mm} \times 13.0\,\text{mm}$), as observed in Fig. 3 (green-colored curve). As can be seen, Ant0 has a single frequency band with impedance bandwidth (VSWR < 3) ranging from 5.30 to 5.61 GHz, which is not enough to cover the whole LTE 46 band (5.150–5.925 GHz). The shaded-green colored column in Table 1 lists the optimized geometrical parameters of the RA, and from it the proposed antenna is obtained to cover both the LTE 42/43 and LTE 46 bands suitable for 5G applications.

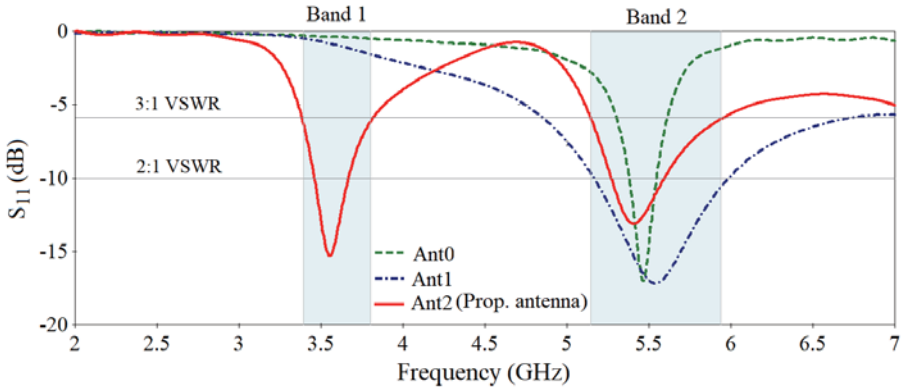

Figure 3. Simulated input reflection coefficient (S_{11}) for antennas (Ant0–Ant2).

Table 2. The final frequency bands, f_r (f_L–f_H) for 3 : 1 and 2 : 1 VSWR of Ant0–Ant2. Unit (in GHz).

Antennas	Band 1		Band 2	
	3 : 1 VSWR	2 : 1 VSWR	3 : 1 VSWR	2 : 1 VSWR
Ant0	-	-	5.47 (5.30–5.61)	5.47 (5.38–5.54)
Ant1	-	-	5.54 (4.86–6.70)	5.54 (5.16–5.98)
Ant2	3.55 (3.38–3.81)	3.55 (3.46–3.66)	5.4 (5.14–5.93)	5.4 (5.27–5.59)

Step 2 (Ant1): In this step, Ant1 is evolved from Ant0 to attain the antenna called a complementary microstrip patch antenna (CMPA) which is presented in this work as an alternative design to the MPA counterpart, named as microstrip slot antenna (MSA). As can be seen in Fig. 2(b), a $50\,\Omega$ microstrip feed line of length L_f and width W_f is printed on the front side of the substrate, and the conductor ground plane cut by rectangular slot of dimensions $W_s \times L_s$ is printed on the back side of the substrate. This slot in the ground represents the radiating element of the MSA where its slot size is responsible for specifying the resonance frequency and impedance bandwidth characteristic. To get $f_r = 5.5\,\text{GHz}$, initially the slot dimensions of the MSA are set equal to the patch dimensions of MPA, that is, $W_s = W_p = 15.7\,\text{mm}$ and $L_s = L_p = 13.0\,\text{mm}$, and all other parameters are kept the same values of Ant0. Then a fine-tune technique offered by CST tool is used for parametric sweeping of the parameters, and as a result Ant1 with optimized geometric parameters (listed as a shaded-blue colored column in Table 1) is achieved with satisfactory desired resonance frequency $f_r = 5.5\,\text{GHz}$, as shown in Fig. 3 (blue-colored curve). As observed from Fig. 3, Ant0 and Ant1 are single-band antennas, and they operate at nearly the same resonance frequency $f_r \cong 5.5\,\text{GHz}$, but more bandwidth is attained by Ant1 (or MSA) than Ant0 (or MPA). Thus, Ant1 has an improvement in impedance bandwidth for both the criteria, reflection coefficient $|S_{11}| < -6\,\text{dB}$ (or 3 : 1 VSWR) and $|S_{11}| < -10$ (or 2 : 1 VSWR) as noticed in Table 2, which covers the whole LTE 46 band. Although MSA covers LTE 46 band, it is not able to work at the LTE 42/43 band. Thus, it is required to modify or add new structure(s) to Ant1 to operate at dual-band frequency range suitable for LTE 42/43 and LTE 46 bands, and its total size remains the same as that used for the previously designed antennas (that is, $18\,\text{mm} \times 18\,\text{mm}$). This is done in the next design step by presenting the proposed antenna (Ant2).

Step 3 (Ant2): In this third and final step of the design procedure, Ant2 is obtained as the proposed antenna, see Fig. 2(c), by adding a parasitic ring-shaped strip resonator of dimensions $W_r \times L_r$ and thickness (t) at a gap distance (g) inside the main slot radiator of Ant1, which is referred as ring MSA (RMSA). The final parameter values of the proposed antenna are specified as a shaded-red colored column in Table 1, and the simulated reflection coefficient result of this designed antenna is shown as a red-colored curve in Fig. 3. As observed from Fig. 3 and the shaded-red colored column in Table 1, the antenna exhibits excellence dual-band behavior for the criterion (VSWR < 3 or $|S_{11}| < -6\,\text{dB}$) in the operating frequency bands: Band 1 of (3.38–3.81 GHz); Band 2 of (5.14–5.93 GHz) with a resonance frequency of 3.55 and 5.4 GHz in the two bands, respectively. Therefore, Ant2 is successfully designed to satisfy the requirements of the 5G smartphones in the LTE bands, and Band 1 and Band 2 cover LTE 42/43 band and LTE 46 band, respectively.

2.3. Performance Evaluation of the Single Antenna Element

This section presents the performance evaluation of three proposed antenna types described in the previous section as evolution steps of designing the proposed single antenna element. These types are MPA (Ant0), MSA (Ant1) and RMSA (Ant2) as presented in Figs. 2(a), (b), and (c), respectively. The microwave simulator CST is used for simulation and performance evaluation of these designed antennas. These performances include surface current distribution and far-field radiation characteristics such as gain, efficiency, 2D and 3D radiation patterns.

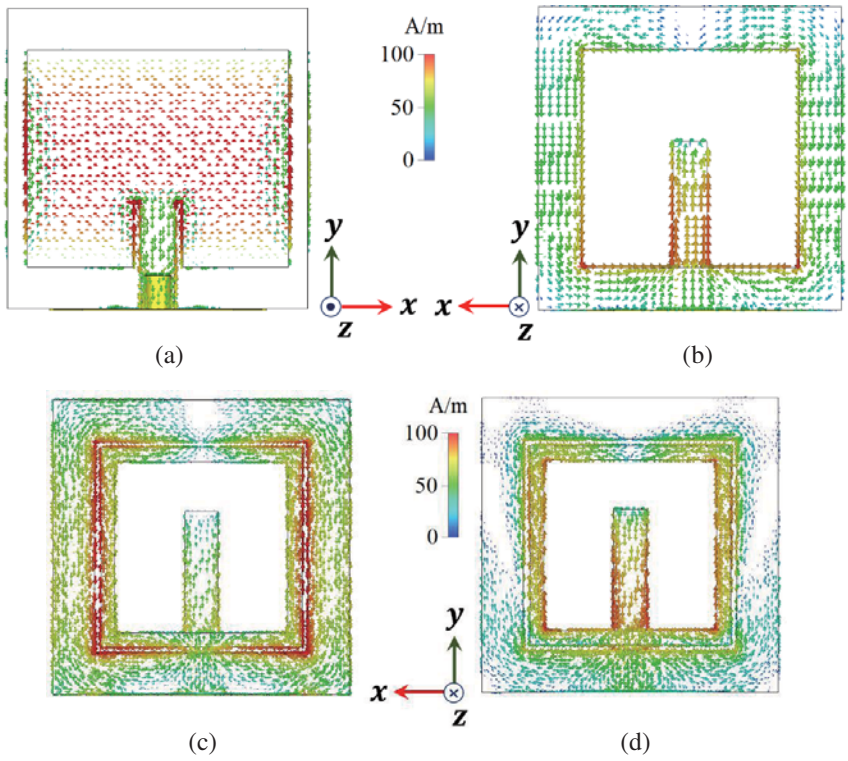

Figure 4. Simulated surface current distributions at (a) 5.5 GHz (for Ant0), (b) 5.5 GHz (for Ant1), (c) 3.55 GHz and (d) 5.4 GHz (for Ant2).

2.3.1. Surface Current Distribution

To understand the working principle of the proposed antennas, the surface current densities at the resonance frequency 5.5 GHz for single band antennas, Ant0 and Ant1, and at 3.5 and 5.5 GHz for dual-band antenna (Ant2) are shown in Figs. 4(a)–(d), respectively. It can be observed from Figs. 4(a) and (b) that at $f_r = 5.5$ GHz, the surface current is highly concentrated at both the MPA (SMA) vertical patch's (slot's) radiator and the microstrip feedline. This behavior of current at the surface of these two antennas demonstrates that they are complement to each other according to the well-known concept named as the Babinet's principle [33, 34]. This principle relates the impedances of the MPA and MSA, Z_{patch} and Z_{slot}, respectively to the intrinsic impedance (η) of the media as:

$$Z_{\text{patch}} Z_{\text{slot}} = \frac{\eta^2}{4} \tag{3}$$

This principle can be verified for the two antennas by plotting their input impedance characteristics as a function of frequency as shown in Fig. 5. It is observed that the real and imaginary parts for the input impedance of the antennas, $\text{Re}(Z_{\text{patch}})$, $\text{Re}(Z_{\text{slot}})$ and $\text{Im}(Z_{\text{patch}})$, $\text{Im}(Z_{\text{slot}})$, at the resonance frequency of 5.5 GHz are 50.35, 54.35 Ω and −17.40, 14.20 Ω, respectively. Moreover, the behavior of $\text{Im}(Z_{\text{patch}})$ curve is purely inductive whereas $\text{Im}(Z_{\text{slot}})$ plot is nearly capacitive.

Figures 4(c) and (d) depict the current distributions in the back and front surface layers of the ring-shaped microstrip slot antenna (RMSA) at the resonance frequencies of 3.55 and 5.4 GHz, respectively. It can be noticed that the surface current is maximally distributed at a gap region around the main slot radiator and a ring resonator when a feeding port is excited by 3.55 GHz, Fig. 4(c), and for exciting the antenna by 5.4 GHz, the maximum current flows at the feedline and parasitic ring structure. Therefore, the employed ring resonator is very active for determining the low band (3.55 GHz), whereas the main slot is responsible for the high band (5.4 GHz).

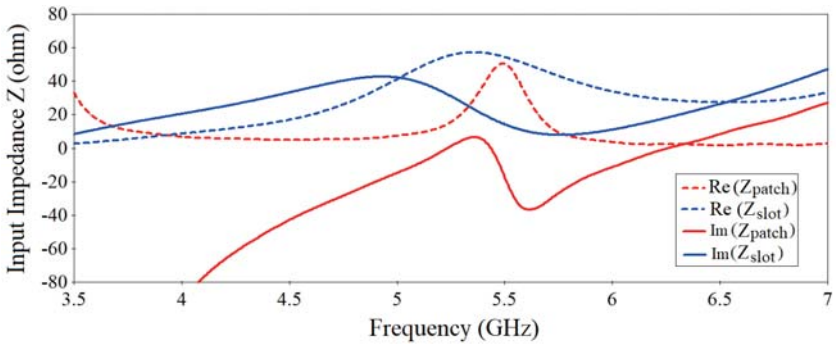

Figure 5. Simulated input impedance Z_{patch} and Z_{slot} of the MPA and MSA, respectively.

2.3.2. Radiation Patterns

The simulated 3D and 2D radiation patterns of Ant0, Ant1, and Ant2 at their resonance frequencies are presented in this section. Before doing that, the concept of Babinet's principle is shown by plotting the E- and H-field components in radiation patterns for the complementary antennas Ant0 and Ant1, which are called respectively as MPA and MSA. Due to Babinet's principle, two antennas are called complementary antennas if the far-fields radiated by them are related by [33]

$$E_{\theta\text{patch}} = H_{\theta\text{slot}}, \quad E_{\phi\text{patch}} = H_{\phi\text{slot}} \tag{4}$$

Figures 6(a) and (c) depict the plots of $E_{\theta\text{patch}}$ and $E_{\phi\text{patch}}$ for MPA, and Figs. 6(b) and (d) show the plots of $H_{\theta\text{slot}}$ and $H_{\phi\text{slot}}$ for MSA, respectively. As can be seen, good results are obtained related to the complementary antennas in terms of E- and H-components validating the Babinet's' principle. Thus, it is better to use MSA than MPA as a single antenna element because of its simple structure,

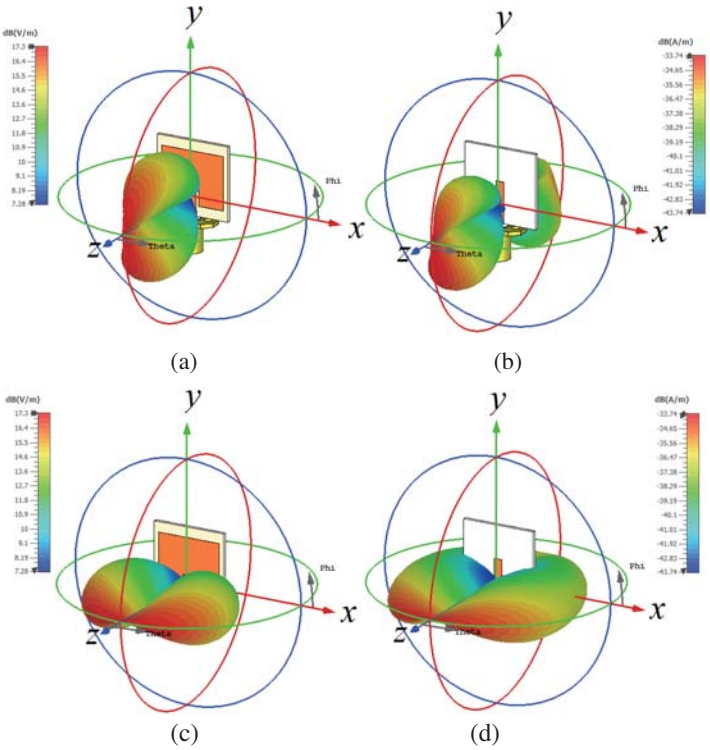

Figure 6. 3D E- and H-field components in radiation patterns at 5.5 GHz for the proposed antennas MPA and SMA. (a) E_θ for MPA. (b) H_θ for MSA. (c) E_ϕ for MPA. (d) H_ϕ for MSA.

and it is radiating element occupying only limited area in the grounded mobile PCB. Hence, in this work the MSA is chosen as a single antenna element to design 5G MIMO antenna array for smartphone applications.

The 3D and 2D radiation patterns of Ant0–Ant2 at their resonance frequencies are illustrated in Figs. 7 and 8, respectively. As shown in Fig. 7, Ant0 has a single-direction of maximum radiation in its front side at the normal axis ($+ve.$ z-axis), whereas Ant1 and Ant2 have a bi-direction of maximum radiation in their front and back sides at the ($+ve.$ and $-ve.$ z-axis). Thus, Ant1 and Ant2 have approximately omnidirectional radiation in xz-plane (normal to the antenna) and nearly null of radiation at y-axis.

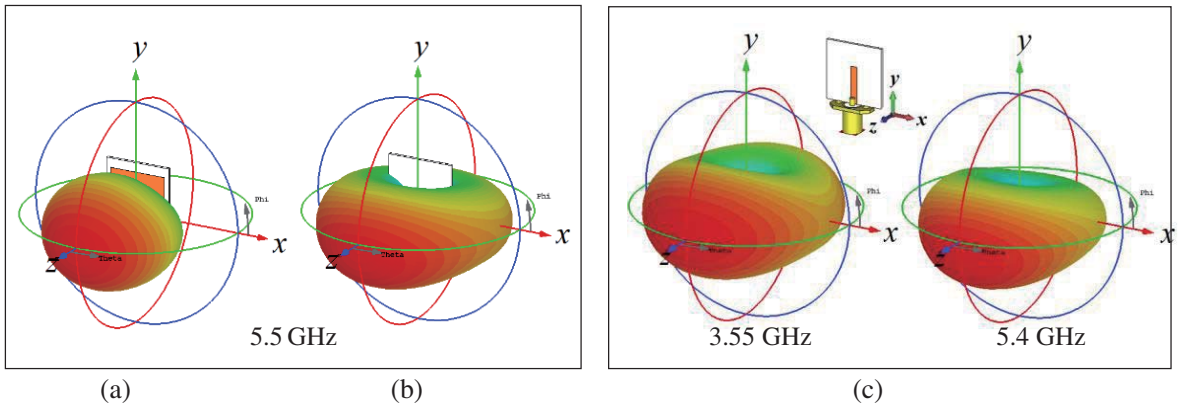

Figure 7. 3D radiation patterns of the proposed antennas: (a) Ant0; (b) Ant1; and (c) Ant2.

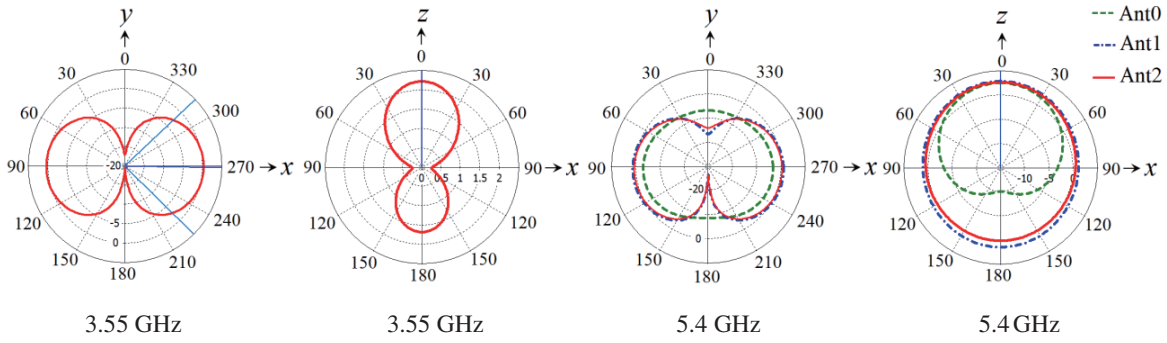

Figure 8. 2D radiation patterns for the proposed antennas, Ant0, Ant1 and Ant2.

Figure 8 demonstrates the simulated radiation patterns, in xy- and xz-planes, for the three antennas at 3.55 GHz and 5.4 GHz. It is seen that the main lobes of radiation in xy-plane (yz-plane) for Ant0 and Ant1 at 5.4 GHz are directed to 0°, 90° and 270° (0°) and 90° and 270° (all direction), respectively. Also, Ant2 has the main lobes of radiation at 3.55 GHz and 5.4 GHz, respectively, in xy-plane (yz-plane) which are oriented to 90° and 270° (0° and 180°) and 90° and 270° (all directions). Thus, Ant2 has good radiation characteristic which leads to better diversity when being used in a 5G MIMO system.

2.3.3. Realized Peak Gain and Efficiency

The peak realized gain and total efficiency of the three antennas are illustrated in Fig. 9. As shown in Figs. 9(a) and (b), Ant0 (Ant1) has lesser (larger) gain and efficiency at the LTE 46 band, and Ant2 has the middle values among the two. Table 3 summaries the gain and efficiency for the antennas at LTE 42/43 band and LTE 46 band. As noticed in Table 3 and Fig. 9, the proposed antenna (Ant2) has an acceptable gain and efficiency in the low and high bands as: 2.24 dB(1.07 $\sim$ 1.85 dB), 83.8%(63.5 $\sim$ 67.1%) and 2.85 dB(1.47 $\sim$ 1.92 dB), 80.5%(55.6 $\sim$ 65.7%)

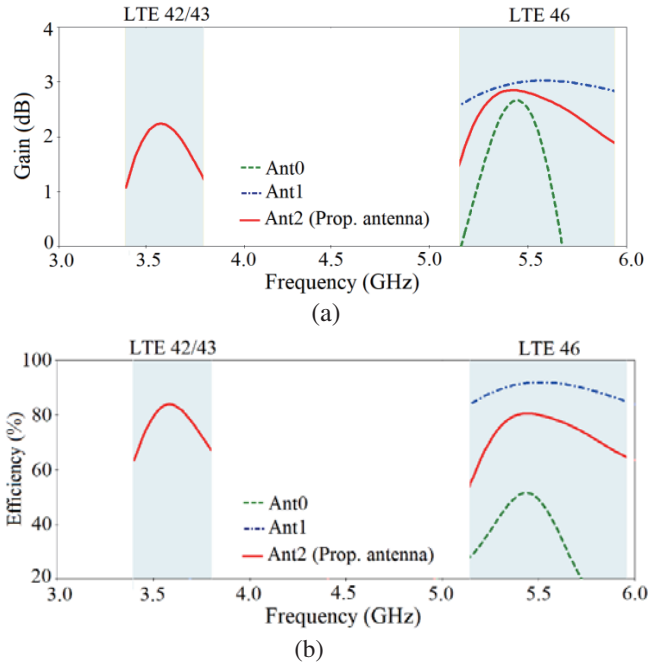

Figure 9. Simulated (a) realized gain and (b) efficiency for the proposed single antenna.

Table 3. The realized peak gain and efficiency at LTE 42/43 band and LTE 46 band for Ant0, Ant1 and Ant2.

Antennas	LTE 42/43 band		LTE 46 band	
	Gain (dB) Max (range)	Efficiency (%) Max (range)	Gain (dB) Max (range)	Efficiency (%) Max (range)
Ant0	-	-	2.66($-0.12 \sim -5.58$)	51.5($28.5 \sim 07$)
Ant1	-	-	3.02($2.56 \sim 2.84$)	92.0($84.2 \sim 85.7$)
Ant2	2.24($1.07 \sim 1.85$)	83.8($63.5 \sim 67.1$)	2.85($1.47 \sim 1.92$)	80.5($55.6 \sim 65.7$)

2.4. Antenna Experimental Result

To appreciate the validity of the attained results, a prototype of the designed antenna is manufactured and measured in microwave laboratory. Photographs of the fabricated prototype and its simulated and measured reflection coefficients are shown in Figs. 10 and 11, respectively. It is seen from Fig. 11 that the antenna covers two bands for using in the LTE 42/43 and LTE 46 bands. Table 4 summaries the simulated and measured bands for the two criteria -10 dB or 2 : 1 VSWR and -6 dB or 3 : 1 VSWR.

Table 4. The simulated and measured frequency bands, f_r (f_L–f_H) for 3 : 1 and 2 : 1 VSWR of the proposed single antenna. Unit (in GHz).

Result	Band 1, LTE 42/43 bands		Band 2, LTE 46 band	
	3 : 1 VSWR	2 : 1 VSWR	3 : 1 VSWR	2 : 1 VSWR
Simulated	3.55 (3.38–3.81)	3.55 (3.46–3.66)	5.40 (5.14–5.93)	5.40 (5.27–5.59)
Measured	3.45, (3.28–3.84) 3.72	3.45, (3.34–3.78) 3.72	5.72 (5.14–> 6.0)	5.72 (5.58–5.82)

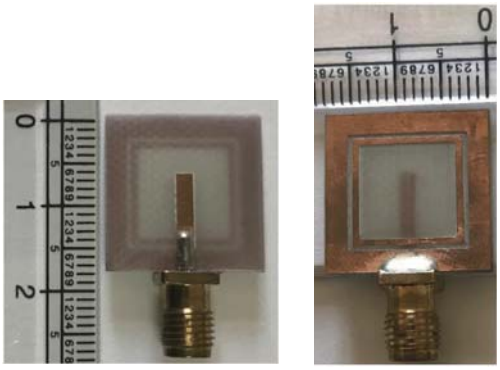

(a) (b)

Figure 10. Picture of the fabricated proposed single antenna element. (a) Top layer and (b) bottom layer.

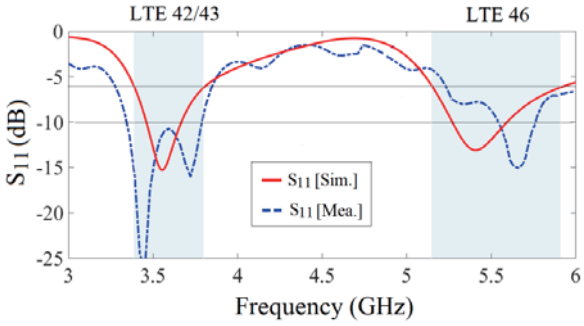

Figure 11. Simulated and measured reflection coefficient of the single antenna.

It is observed that for −6 dB or 3:1 VSWR simulated and measured frequency bands are: band 1 of (3.38–3.81 GHz) and (3.28–3.84 GHz); band 2 of (5.14 greater than 6.0 GHz) and (5.58–5.82 GHz), respectively. Thus, the proposed single antenna is suitable to be used as a single antenna element in the 5G MIMO antenna system for mobile devices.

3. THE MIMO SMARTPHONE ANTENNA CONFIGURATION AND CHARACTERISTICS

3.1. The 8 × 8 MIMO Antenna Configuration

The configuration of the proposed designed dual-band MIMO smartphone antenna is illustrated in Fig. 12. As can be seen, it comprises eight RMSA elements, four (Ant1, Ant4, Ant5, and Ant8) arranged in parallel (at the 4 corners) and the other four (Ant2, Ant3, Ant6 and Ant7) horizontally (at the middle) oriented in the mobile system board. The FR-4 substrate, with a height of $h_{sub} = 0.8$ mm, is used as a low-cost material with standard size dimensions of $150 \times 80\,\text{mm}^2$ for the smartphone mainboard.

Figure 13 displays the simulated S-parameters (reflection and transmission coefficients) of the designed 8-element MIMO antenna system. As observed from Fig. 13(a), Ant1 to Ant8 have exhibited good reflection coefficients S_{nn} ($n = 1, \ldots, 8$), better than −6 dB, and the transmission coefficients S_{1n} between Ant1 and the other seven antenna elements are sufficient (better than −10 dB) over the working frequency range (2.5–6.5 GHz).

3.2. The Characteristic of MIMO Antenna System

The characteristic of designed MIMO antenna system is evaluated by necessary parameters, such as far-field performance, gain, efficiency, radiation patterns, envelope correlation coefficient (ECC), and Total Active Reflection Coefficient (TARC).

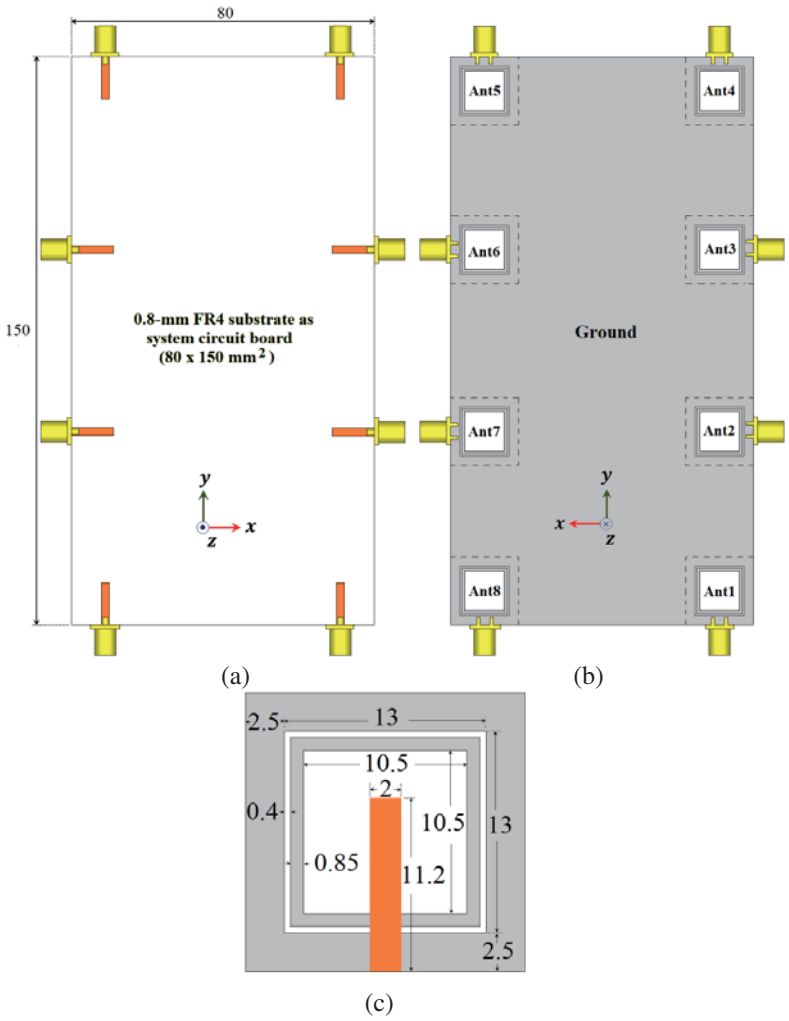

Figure 12. Designed smart-phone antenna configuration (a) front view, (b) back-view and (c) single antenna element.

3.2.1. The Realized Peak Gain, Efficiency, and Radiation Patterns

The simulated gain and efficiency for the MIMO system are depicted in Fig. 14. It is seen from Figs. 14(a) and (b) that the radiation gains and efficiencies for the eight antenna elements (Ant1 to Ant8) are more than 3 dB and 65% (1.5 dB and 60%). Thus, acceptable gains and efficiencies are obtained for the radiation antenna elements at both the bands, LTE 43 and LTE 46.

As shown in Fig. 15, which displays front-views of the 3D radiation patterns for each one of the eight antenna elements (Ant1–Ant8) at two frequencies (3.7 and 5.4 GHz, Figs. 15(a) and (b), respectively), all sides of the smartphone mainboard have been covered by these radiations. Therefore, the designed MIMO system shows excellent radiation coverage due to its supporting different polarizations which make it greatly convenient for using in future 5G smartphone applications. Furthermore, each antenna element of the MIMO system provides a nearly omnidirectional radiation in H-plane and bidirectional radiation in E-plane at the two aforementioned frequencies, as shown in Fig. 16.

3.2.2. The ECC and TARC

To make certain that the MIMO antenna is able to work appropriately, ECC and TARC are considered two important parameters that should be used for sufficiently describing the degree of correlation between antenna elements and properly estimating the whole radiation performance of

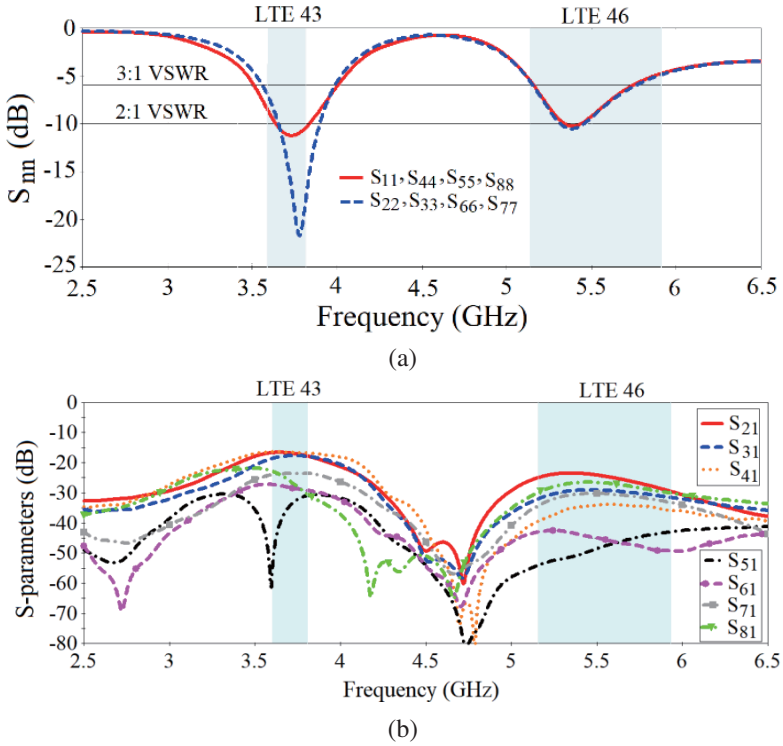

Figure 13. Simulated S-parameters of the 8-element MIMO antenna system. (a) Reflection coefficients and (b) transmission coefficients.

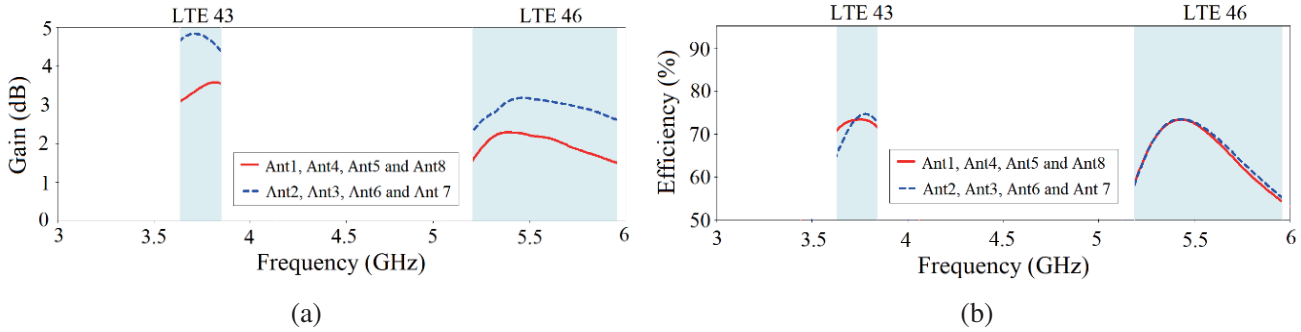

Figure 14. Simulated gain (a) and efficiency (b) for the proposed 8-element MIMO antenna system.

MIMO system [35, 36]. $ECC(i, j, N)$ between two antenna elements i and j and TARC characteristics of N-element MIMO system can be computed from the S-parameters employing the following two formulas as:

$$ECC(i,j,N) = \left| \frac{\sum_{n=1}^{N} S_{i,n}^{*} S_{n,j}}{\left| \prod_{k=i,j} \left(1 - \sum_{n=1}^{N} S_{k,n}^{*} S_{n,k} \right) \right|^{1/2}} \right|^{2} \tag{5}$$

$$TARC = \frac{\sqrt{|s_{11} + s_{12} + \ldots + s_{1n}|^2 + |s_{21} + s_{22} + \ldots + s_{2n}|^2 + \ldots + |s_{n1} + s_{n2} + \ldots + s_{nn}|^2}}{\sqrt{N}} \tag{6}$$

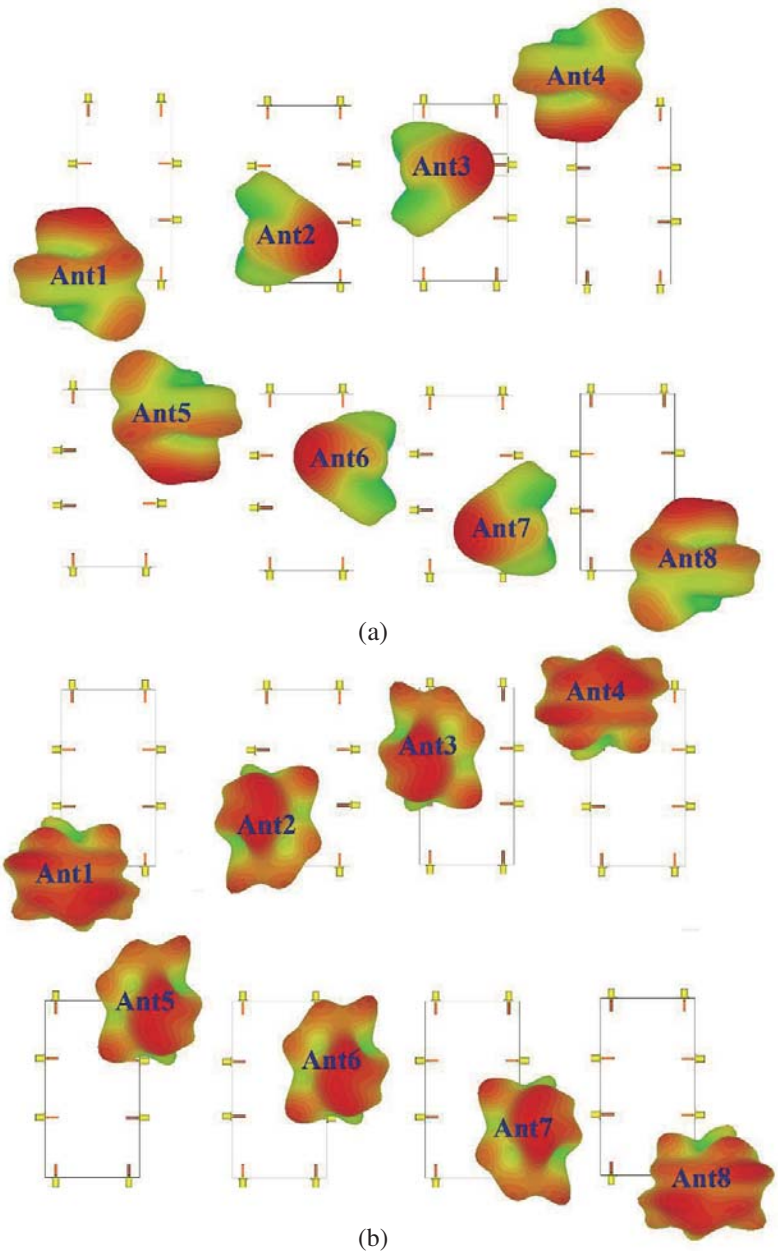

Figure 15. 3D antenna radiation patterns at (a) 3.7 GHz and (b) 5.4 GHz for the 8-antenna MIMO system.

Figure 17 displays the computed ECC and TARC characteristics from simulated S parameters of the MIMO antenna design. As clarified from figures, the calculated ECC (1, 2, 8), ..., ECC (2, 3, 8) and TARC over the two bands of interest, LTE 43 band and LTE 46 band, are less than 0.01 and -6 dB, respectively. Thus, the MIMO system can provide better performance in terms of total efficiency, radiation, ECC, and TARC besides polarization diversity and dual-band characteristics that make it appropriate for 5G smartphone antenna designs in LTE bands.

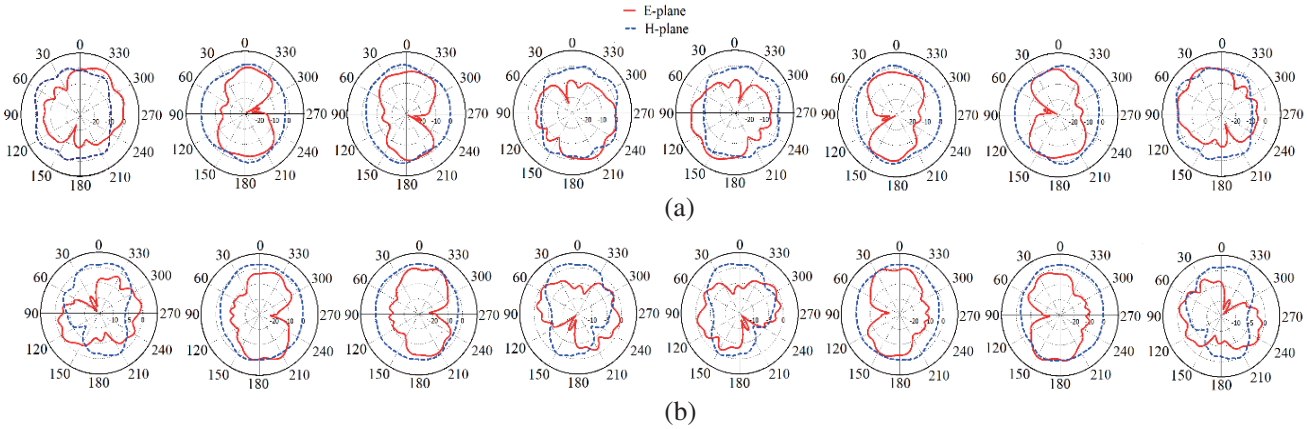

Figure 16. Simulated 2D antenna radiation patterns at (a) 3.7 GHz and (b) 5.7 GHz for the 8-antenna MIMO system, Ant1 (left) to Ant8 (right).

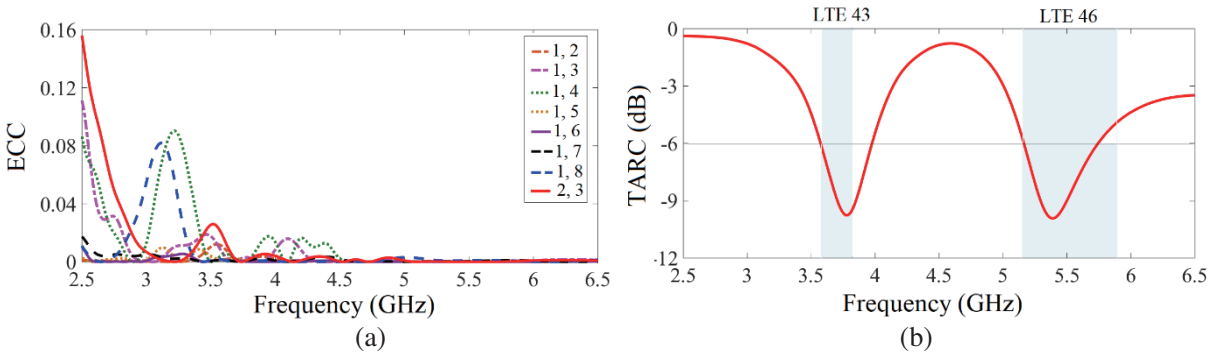

Figure 17. Simulated (a) ECC and (b) TARC results.

Table 5. Performance comparison between the proposed MIMO antenna array and reported ones.

Ref.	MIMO order	Ground size (mm^2)	Bandwidth (MHz)	Efficiency (%)	ECC (dB)
[21]	10	150×80	3400–3800 5150–5925 (−6 dB)	42–65 (low band) 62–82 (high band)	≤ 0.15
[24]	10	150×80	3400–3800 5150–5925 (−6 dB)	55.5–69.1(low band) 48.9–62.8(high band)	≤ 0.10
[25]	8	140×70	3400–3800 5150–5925 (−6 dB)	51–59 (low band) 62–80 (high band)	≤ 0.08
[26]	8	150×75	3400–3600 (−10 dB) 5150–5925 (−6 dB)	50–56 (low band) 53–65 (high band)	≤ 0.10
[27]	8 (low band) 6 (high band)	150×80	3400–3600 5150–5925 (−6 dB)	41–82 (low band) 47–79 (high band)	≤ 0.15
proposed	8	150×80	3600–3800 5150–5925 (-6 dB)	65–73 (low band) 54–74 (high band)	≤ 0.05

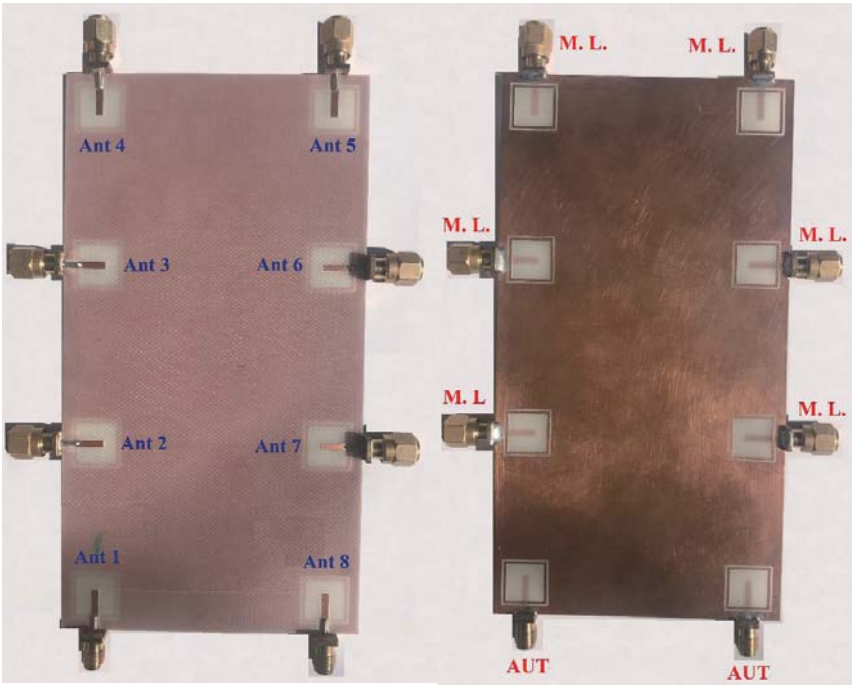

(a) (b)

Figure 18. Picture of the fabricated proposed 8-element MIMO antenna system, (a) top layer and (b) bottom layer. Herein, the SMA connectors for Ant1 and Ant8 of this prototype are considered the AUT (antenna under test) were connected to VNA for measuring the S-parameters and the other six antennas (Ant2–Ant7) were connected to the 50-Ohm matched load (M.L.).

4. THE MEASURED RESULTS OF 8-ELEMENT MIMO SYSTEM

The proposed smartphone antenna is fabricated on a low-cost FR4 substrate with an overall dimension of $80 \times 150 \times 0.8\,\text{mm}^3$, and its S-parameters are measured in the Microwave Laboratory at the Al-Nahrain University. Front and back views of the prototype are shown in Figs. 18(a) and 18(b), respectively. During the measurement, a $50\,\Omega$ matched load (M.L.) is used for the antenna element not under test for avoiding its influences on the result, and the element antenna(s) under test (AUT) is(are) connected to the VNA via SMA connectors. Due to symmetry of the 8-element MIMO array, the simulated and measured S-parameters (reflection coefficients: S_{11} and S_{22} and transmission coefficients: S_{21}, S_{23} and S_{27}) of the fabricated prototype are only the curves depicted in Figs. 19(a) and 19(b), respectively.

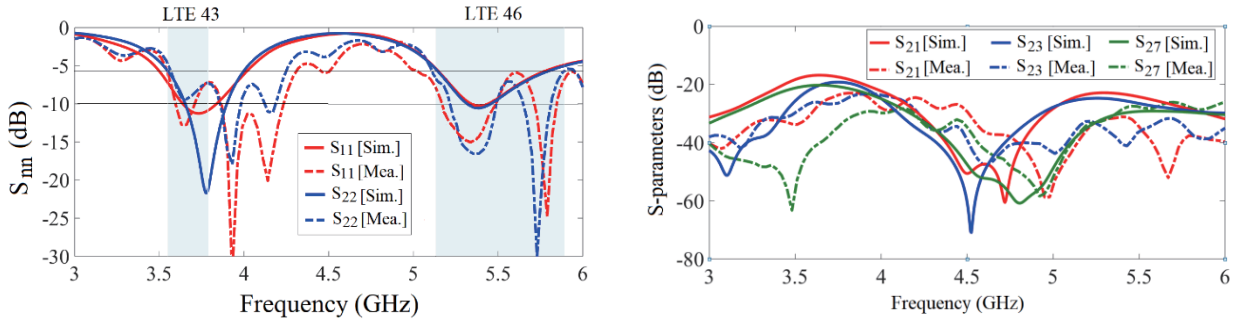

(a) (b)

Figure 19. Simulated and measured S-parameters of the 8-element MIMO antenna system. (a) Reflection coefficients and (b) transmission coefficients.

As observed, the slots and strip-ring resonators attain good reflection coefficients with appropriate −6 dB impedance bandwidth covering both the LTE 43/46 bands and good isolation performance over the whole bands of interest. The simulated and measured results are in good agreement, and some deviations between them are due to the errors during the fabrication, soldering SMAs to the smartphone mainboard, and measurement processes.

Table 5 summarizes and compares the performance of presented smartphone antenna with that of the recently reported ones [21, 24–27]. It can be noticed that the proposed 8-antenna MIMO array, compared with the other, can work within both LTE band 43 and LTE band 46. Also, the MIMO antenna system provides better performance in terms of ECC, less than 0.05. Moreover, good efficiency with enhancement in pattern and polarization diversity characteristics, covering different directions of the PCB mainboard, are achieved over the two specified bands. Hence, the proposed MIMO antenna can be used for 5G smartphone applications.

5. CONCLUSION

A smartphone antenna design for 5G MIMO communications has been proposed in this paper. The antenna configuration comprises eight single antenna elements which are called strip-ring shaped microstrip slot antenna (RMSA). This antenna is successfully designed from its counterpart microstrip patch antenna (MPA) using the theory of Babinet's principle, and its prototype is fabricated and measured demonstrating that the LTE 42/43/46 bands have been achieved. In addition, a prototype of the MIMO antenna smartphone comprises eight RMSAs is manufactured and measured. The measured results display that all the antenna elements exhibit good impedance bandwidth covering LTE 43 band (3.6–3.8 GHz) and LTE 46 band (5.150–5.925 GHz) with better isolation, good ECC, and TARC results besides an acceptable gain and antenna efficiency over the bands of interest. Thus, the attained results demonstrate that the proposed MIMO antenna design can be used for the future 5G MIMO smartphones.

ACKNOWLEDGMENT

The authors would like to thank Dr. Ghassan N. Jawad from the University of Baghdad for providing the measurement results.

REFERENCES

1. Parchin, N. O., H. J. Basherlou, M. Alibakhshikenari, Y. O. Parchin, Y. I. Al-Yasir, R. A. Abd-Alhameed, and E. Limiti, "Mobile-phone antenna array with diamond-ring slot elements for 5G massive MIMO Systems," *Electronics*, Vol. 8, No. 5, 1–17, 2019.
2. Rahman, M., M. N. Jahromi, S. S. Mirjavadi, and A. M. Hamouda, "Bandwidth enhancement and frequency scanning array antenna using novel UWB filter integration technique for OFDM UWB radar applications in wireless vital signs monitoring," *Sensors*, Vol. 18, 3155, 2018
3. Rahman, M., M. N. Jahromi, S. S. Mirjavadi, and A. M. Hamouda, "Resonator based switching technique between ultra wide band (UWB) and single/dual continuously tunable-notch behaviors in UWB radar for wireless vital signs monitoring," *Sensors*, Vol. 18, 3330, 2018.
4. Rahman, M., M. N. Jahromi, S. S. Mirjavadi, and A. M. Hamouda, "Compact UWB band-notched antenna with integrated bluetooth for personal wireless communication and UWB Applications," *Electronics*, Vol. 8, 158, 2019.
5. Park, J.-D., M. Rahman, and H. N. Chen, "Isolation enhancement of wide-band MIMO array antennas utilizing resistive loading," *IEEE Access*, Vol. 7, 81020–81026, 2019
6. Ai-Hadi, A. A., J. Ilvonen, R. Valkonen, and V. Viikari, "Eight-element antenna array for diversity and MIMO mobile terminal in LTE 3500 band," *Microw. Opt. Technol. Lett.*, Vol. 56, 1323–1327, Jun. 2014.
7. Li, M.-Y., Y. L. Ban, Z. Q Xu, G. Wu, C. Sim, K. Kang, and Z. F. Yu, "Eightport orthogonally dual-polarized antenna array for 5G smartphone applications," *IEEE Trans. Antennas Propag.*, Vol. 64, No. 9, 3820–3830, Sep. 2016.

8. Li, M.-Y., Z.-Q. Xu, Y.-L. Ban, C.-Y.-D. Sim, and Z.-F. Yu, "Eight-port orthogonally dual-polarised MIMO antennas using loop structures for 5G smartphone," *IET Microw., Antennas Propag.*, Vol. 11, 1810–1816, Dec. 2017.
9. Li, M.-Y., Y. L. Ban, Z. Q. Xu, J. Guo, and Z. F. Yu, "Tri-polarized 12-antenna MIMO array for future 5G smartphone applications," *IEEE Access*, Vol. 6, 6160–6170, Jan. 2018.
10. Wong, K.-L., C.-Y. Tsai, and J.-Y. Lu, "Two asymmetrically mirrored gap-coupled loop antennas as a compact building block for eight-antenna MIMO array in the future smartphone," *IEEE Trans. Antennas Propag.*, Vol. 65, No. 4, 1765–1778, Apr. 2017.
11. Wong, K. L., B. W. Lin, and W. Y. Li, "Dual-band dual inverted F/loop antennas as a compact decoupled building block for forming eight 3.5/5.8-GHz MIMO antennas in the future smartphone," *Microw. Opt. Technol. Lett.*, Vol. 59, 2715–2721, Nov. 2017.
12. Xu, H., H. Zhou, S. Gao, H. Wang, and Y. Cheng, "Multimode decoupling technique with independent tuning characteristic for mobile terminals," *IEEE Trans. Antennas Propag.*, Vol. 65, No. 12, 6739–6751, Dec. 2017.
13. Ren, Z. and A. Zhao, "Dual-band MIMO antenna with compact self-decoupled antenna pairs for 5G mobile applications," *IEEE Access*, Vol. 7, 82288–82296, 2019.
14. Wong, K.-L., J.-Y. Lu, L.-Y. Chen, W.-Y. Li, and Y.-L. Ban, "8-antenna and 16-antenna arrays using the quad-antenna linear array as a building block for the 3.5-GHz LTE MIMO operation in the smartphone," *Microw. Opt. Technol. Lett.*, Vol. 58, 174–181, Jan. 2016.
15. Guo, J. L., L. Cui, C. Li, and B. H. Sun, "Side-edge frame printed eight-port dual-band antenna array for 5G smartphone applications," *IEEE Trans. Antennas Propag.*, Vol. 66, No. 12, 7412–7417, Dec. 2018.
16. Li, Y., C.-Y.-D. Sim, Y. Luo, and G. Yang, "Metal-frame-integrated eight-element multiple-input multiple-output antenna array in the long term evolution bands 41/42/43 for fifth generation smartphones," *Int. J. RF Microw. Comput. — Aided Eng.*, Vol. 29, No. 1, Jan. 2019, Art. No. e21495.
17. Zhao, A. and Z. Ren, "Multiple-input and multiple-output antenna system with self-isolated antenna element for fifth-generation mobile terminals," *Microw. Opt. Technol. Lett.*, Vol. 61, 20–27, Jan. 2019.
18. Zhao, A. and Z. Ren, "Size reduction of self-isolated MIMO antenna system for 5G mobile phone applications," *IEEE Antennas Wireless Propag. Lett.*, Vol. 18, No. 1, 152–156, Jan. 2019.
19. Sun, L. B., H. Feng, Y. Li, and Z. Zhang, "Compact 5G MIMO mobile phone antennas with tightly arranged orthogonal-mode pairs," *IEEE Trans. Antennas Propag.*, Vol. 66, No. 11, 6364–6369, Nov. 2018.
20. Hassan, N. and X. Fernando, "Massive MIMO wireless networks: An overview," *Electronics*, Vol. 6, 63, 2017.
21. Li, Y., C.-Y.-D. Sim, Y. Luo, and G. Yang, "Multiband 10-antenna array for sub-6 GHz MIMO applications in 5-G smartphones," *IEEE Access*, Vol. 6, 28041–28053, 2018.
22. Roy, S., S. Ghosh, and U. Chakarborty, "Compact dual wide-band four/eight elements MIMO antenna for WLAN applications," *International Journal of RF and Microwave Computer-Aided Engineering*, e21749, 2019.
23. Qin, Z., W. Geyi, M. Zhang, and J. Wang, "Printed eight-element MIMO system for compact and thin 5G mobile handset," *Electronics Letters*, Vol. 52, No. 6, 416–418, 2016.
24. Li, Y. and G. Yang, "Dual-mode and triple-band 10-antenna handset array and its multiple-input multiple-output performance evaluation in 5G," *International Journal of RF and Microwave Computer-Aided Engineering*, Vol. 29, No. 2, e21538, 2019.
25. Li, J., X. Zhang, Z. Wang, X. Chen, J. Chen, Y. Li, and A. Zhang, "Dual-band eight-antenna array design for MIMO applications in 5G mobile terminals," *IEEE Access*, Vol. 7, 71636–71644, 2019.
26. Zou, H., Y. X. Li, C.-Y.-D. Sim, and G. L. Yang, "Design of 8×8 dual-band MIMO antenna array for 5G smartphone applications," *Int. J. RF Microw. Comput. — Aided Eng.*, Vol. 28, Nov. 2018, Art. No. e21420.

27. Li, Y. X., C.-Y.-D. Sim, Y. Luo, and G. L. Yang, "12-port 5G massive MIMO antenna array in sub-6 GHz mobile handset for LTE bands 42/43/46 applications," *IEEE Access*, Vol. 6, 344–354, 2018.
28. Chaudhari, A. A., V. Jadhav, S. U. Kharche, and R. K. Gupta, "Compact dual-band MIMO antenna with high isolation for 3/4G, Wi-Fi, bluetooth, Wi-MAX and WLAN applications," *Progress In Electromagnetic Research Symposium (PIERS)*, 112–115, Aug. 8–11, 2016.
29. Ran, X., J. Wei, and Z. Yu, "Design of a dual-polarization dual-band MIMO antenna for wireless applications," *International Conference on Modeling, Simulation and Optimization Technologies and Applications (MSOTA 2016)*, 2016.
30. Yang, L., H. Xu, J. Fang, and T. Li, "Four-element dual-band MIMO antenna system for mobile phones," *Progress In Electromagnetics Research*, Vol. 60, 47–56, 2015.
31. Jan, M. A., D. N. Aloi, and M. S. Sharawi, "A 2×1 compact dual band MIMO antenna system for wireless handheld terminals," *IEEE Radio and Wireless Symposium*, 23–26, 2012.
32. Yang, L., J. Fang, and T. Li, "Compact dual-band MIMO antenna system for mobile handset application," *IEICE Transactions on Communications*, Vol. 98, 2463–2469, 2015.
33. Balanis, C. A., *Antenna Theory: Analysis and Design*, 4th Edition, John Wiley & Sons, 2016.
34. Rahman, M., D.-S. Ko, and J.-D. Park, "A compact multiple notched ultra-wide band antenna with an analysis of the CSRR-to-CSRR coupling for portable UWB applications," *Sensors*, Vol. 17, 2174, 2017.
35. Naji, D. K., "Design of a compact orthogonal broadband printed MIMO antennas for 5-GHz ISM band operation," *Progress In Electromagnetics Research B*, Vol. 64, 47–62, 2015.
36. Chae, S. H., S.-K. Oh, and S.-O. Park, "Analysis of mutual coupling, correlations, and TARC in WiBro MIMO array antenna," *IEEE Antennas and Wireless Propagation Letters*, Vol. 6, 2007.